JSS Focus Issue on Visible and Infrared Phosphor Research and Applications

Red-Shifted Absorption of a Mn^{4+}-Doped Germanate Phosphor by Crystal Distortion

Tae Gil Lim, Yong Nam Ahn, Hyun Woo Park, and Jae Soo Yoo[z]

School of Chemical Engineering and Materials Science, Chung-Ang University, Dongjak-gu, Seoul 06974, Korea

A Mn^{4+}-doped germanate red-emitting phosphor, in which TiO_2 is partially substituted for GeO_2, was synthesized by a solid-state reaction. The proportional composition of the compound was $3.5MgO\text{-}Ge_{1-x}Ti_xO_2\text{-}0.5MgF_2:Mn^{4+}$. The main X-ray diffraction peak exhibited a gradual shift to lower angles depending on the synthesis temperature and the extent of Ti substitution. Substitution of GeO_2 with TiO_2 yielded a redshift of the broad excitation band (380–500 nm), which resulted from the $^4A_2 \rightarrow {}^4T_2$ transition of Mn^{4+}. Compared with the sample containing only GeO_2, the relative luminescence of the sample in which GeO_2 was partially replaced with TiO_2 was increased by 19.3% for excitation at 450 nm.

 [DOI: 10.1149/2.0241801jss]

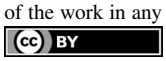

Manuscript submitted August 28, 2017; revised manuscript received October 6, 2017. Published November 4, 2017. *This paper is part of the JSS Focus Issue on Visible and Infrared Phosphor Research and Applications.*

Commercial white light-emitting diodes (WLEDs) use a combination of an InGaN blue chip and a YAG:Ce^{3+} yellow phosphor.[1,2] White light that lacks red light, which is simply a combination of yellow and blue, has a high color temperature in the 4000–8000 K range and a poor color-rendering index (CRI). In particular, the R9 value is low, which decreases usability. Adding red phosphors to packaged WLEDs has been suggested to solve the "low R9" problem.[3] Several studies have focused on red phosphors, using Eu^{3+}, Eu^{2+}, and Mn^{4+} as activators.

The $Y_2O_3:Eu^{3+}$ phosphor absorbs strongly at 259 nm and emits red light at 610 nm. As there is little spectral overlap with blue or near ultraviolet light, this phosphor is unsuitable for use with commonly used InGaN blue chips.[4] $Sr_{1-x}Ca_xS:Eu^{2+}$ phosphors exhibit limitations such as high moisture sensitivity and nondesirable generation of gaseous H_2S during decomposition. Some studies have attempted to overcome these problems.[5,6] Eu^{2+}-doped oxynitride phosphors, such as $Sr_2Si_3O_2N_4:Eu^{2+}$[7] and $Ca_{15}Si_{20}O_{10}N_{30}:Eu^{2+}$,[8] have also been studied.

Nitride series phosphors with excellent thermal stability, such as $M_2Si_5N_8:Eu^{2+}$ (M = Ca, Sr, Ba)[9] and $CaAlSiN_3:Eu^{2+}$,[10] have also been examined. Production of the $CaAlSiN_3:Eu^{2+}$ phosphor, usually requires high temperatures (above 1800°C) and high pressure (0.5 MPa). Red-emitting phosphors, such as $Sr_2Si_5N_8:Eu^{2+}$ and $CaAlSiN_3:Eu^{2+}$, also absorb light in the green region of the visible spectrum. Therefore, when these phosphors are used with fluorescent materials that emit green light, reabsorption occurs, which reduces efficiency.[11]

To solve the above reabsorption problem, phosphors that do not have excitation bands in the green region are used, such as Mn^{4+} in the octahedral crystal field .[12–14] Several studies have attempted to synthesize red phosphors using Mn^{4+}, which is a transition metal, without using rare earths by doping aluminates, titanates, zirconates, germanates, and fluorides. Mn^{4+}-doped phosphors include compounds such as $Sr_4Al_{14}O_{25}:Mn^{4+}$,[15] $Li_2MgTiO_4:Mn^{4+}$,[16] $Li_2MgZrO_4:Mn^{4+}$,[17] $Li_2MgGeO_4:Mn^{4+}$,[18] $K_2Ge_4O_9:Mn^{4+}$,[19] $Li_3RbGe_8O_{18}:Mn^{4+}$,[20] and $K_2SiF_6:Mn^{4+}$.[21] Another Mn^{4+}-doped phosphor that emits at 658 nm, i.e., $3.5MgO\text{-}GeO_2\text{-}0.5MgF_2:Mn^{4+}$ (MGF:Mn^{4+}), was reported in the 1950s.[22] The MGF:Mn^{4+} phosphor does not absorb green light, but strongly absorbs near-ultraviolet light and also partially absorbs blue light. While the absorption of this phosphor at 418 nm is strong, weak absorption occurs at 450 nm, which is the blue wavelength that is mainly used for light-emitting diode (LED) chips. Intensive studies have been carried out to improve the MGF:Mn^{4+} luminescence characteristics. For example, partial replacement of MgO with alkaline-earth fluorides[23] or partial replacement of GeO_2 with Al_2O_3 have been attempted.[24] Recently, the Nichia group has filed a patent, US 9653658 B2, which replaces various components in the MGF:Mn^{4+} phosphor.

Here, we report the red-shifted excitation spectra of a Mn^{4+}-doped germanate deep-red phosphor. Luminescence improved following the partial replacement of GeO_2 with TiO_2 in MGF:Mn^{4+} deep-red phosphors. We studied the effects of this replacement on the structural and photoluminescence emission/excitation (PL/PLE) properties of the phosphor. In this work, we also try to understand how crystal distortion resulting from partial replacement of GeO_2 with TiO_2 leads to a redshift of the $^4A_2 \rightarrow {}^4T_2$ absorption band of Mn^{4+}, which is very important for device applications.

Experimental

Mn^{4+}-doped phosphors, $3.5MgO\text{-}Ge_{1-x}Ti_xO_2\text{-}0.5MgF_2:Mn^{4+}$ (x = 0, 0.05, 0.1, 0.15, 0.2, or 0.25), were obtained by solid-state synthesis using MgO, MgF_2, GeO_2, TiO_2, and Mn_2O_3 as starting materials. In addition, a small amount of SrF_2 was used as a flux.[23] The Mn^{4+} ion concentration was fixed at 1 mol%. The synthesis temperature was controlled while changing x (x = 0, 0.05, 0.1, 0.15, 0.2, or 0.25), which determined the Ti/Ge ratio. First, the starting materials were mixed in isopropyl alcohol (IPA) at 25°C and oven-dried at 80°C for 4 h. The resulting mixtures were transferred into an alumina crucible and loosely sealed using an alumina crucible cover. The mixed powders were calcined in a furnace at 1100 or 1250°C for 7 h. The obtained phosphors were ground in a mortar. The samples were analyzed without any other post-treatment processes.

The synthesized phosphors were characterized by powder X-ray diffraction (XRD, Bruker, New D8-Advance-AXS, 40 kV and 40 mA) using Cu K_α radiation to identify the phase and crystal structure. Careful measurements for each sample have been made for reducing the measurement error and the repeatability was confirmed.

The PL and PLE spectra were recorded at room temperature using a photomultiplier tube and a xenon lamp (PSI, Korea). The absorption ratios and the internal quantum efficiencies of the synthesized phosphors were obtained using a $BaSO_4$-coated integrating sphere with the photomultiplier tube and the xenon lamp (PSI, Korea).

Results and Discussion

Figure 1 shows the XRD patterns of the samples with different compositions obtained at different synthesis temperatures. The synthesized samples had compositions of $3.5MgO\text{-}Ge_{1-x}Ti_xO_2\text{-}0.5MgF_2:Mn^{4+}$. The "1100°C_MGF" sample, which did not contain TiO_2, was synthesized at 1100°C using MgO, MgF_2, and GeO_2. On

[z]E-mail: jsyoo@cau.ac.kr

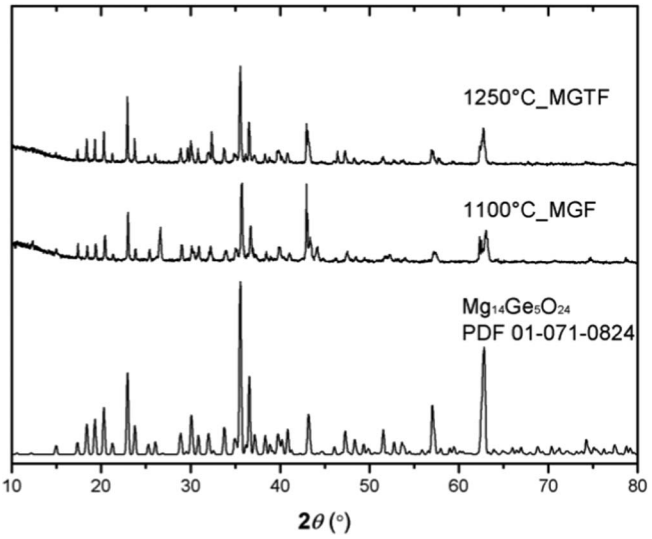

Figure 1. XRD patterns of samples prepared with and without Ti substitution at different synthesis temperatures (1250°C_MGTF and 1100°C_MGF, respectively) and the reference $Mg_{14}Ge_5O_{24}$ phase.

the other hand, the "1250°C_MGTF" sample, in which GeO_2 was partially substituted with TiO_2, was synthesized at 1250°C using MgO, MgF_2, GeO_2, and TiO_2. The Ge/Ti ratio in the 1250°C_MGTF sample was 0.8/0.2. Indexing the XRD patterns revealed that these two samples comprise mostly $Mg_{14}Ge_5O_{24}$ (PDF 01-071-0824). XRD peaks corresponding to some impurities, such as SrF_2, Sr_2MgGeO_7, $SrTiO_3$, and MgO were also observed, but these peaks, in general, were weak. With the exception of some of the impurity phases, there were no significant differences between the XRD profiles of the two synthesized samples.

Figures 2a and 2b show comparisons of the absorption and emission properties of the 1100°C_MGF and 1250°C_MGTF samples. The absorption and emission properties were recorded using a photomultiplier tube and a xenon lamp. Figure 2a shows the PLE spectra (emission at 660 nm) in the range of 200–500 nm. The shape of the absorption spectrum is similar, but not exactly overlapping. At wavelengths less than 420 nm, the 1100°C_MGF sample exhibits relatively higher absorption. At wavelengths near 420 nm, the two samples exhibit similar absorption. As wavelengths above 420 nm, including 450 nm, the 1250°C_MGTF sample exhibits relatively higher absorption. When the synthesis temperature was increased from 1100°C to 1250°C and some GeO_2 was replaced with TiO_2, the PLE spectrum was slightly red-shifted.

Figure 2b shows the PL spectra for excitation at 450 nm, which is similar to the emission wavelength of InGaN blue LED chips. For the 1100°C_MGF sample, the peak wavelength was 660 nm, the dominant wavelength was 634.6 nm, the full width at half maximum was 16.8 nm, and the relative luminescence was 16.1. For the 1250°C_MGTF sample, the peak wavelength was 660 nm, the dominant wavelength was 635.6 nm, the full width at half maximum was 17.6 nm, and the relative luminescence was 19.2, which is 19.3% higher than the 1100°C_MGF sample. We measured the absorption ratios and the internal quantum efficiencies of the 1250°C_MGTF sample using a $BaSO_4$-coated integrating sphere with the photomultiplier tube and the xenon lamp. The internal quantum efficiency of the obtained phosphor (1250°C_MGTF sample) was 45.36%, and the absorption ratio at 450 nm was 50.16%. $BaSO_4$ powders with a reflectivity of ~100% in the visible region were used as a standard for calculating the excitation source spectrum. Measurements of internal quantum efficiency and the absorption ratio were carried out using excitation at 450 nm. The internal quantum efficiency of the phosphor was calculated using the following equation:

$$\eta_i = (\int \lambda \cdot P(\lambda)\, d\lambda) / (\int \lambda \{E(\lambda) - R(\lambda)\}\, d\lambda) \quad [1]$$

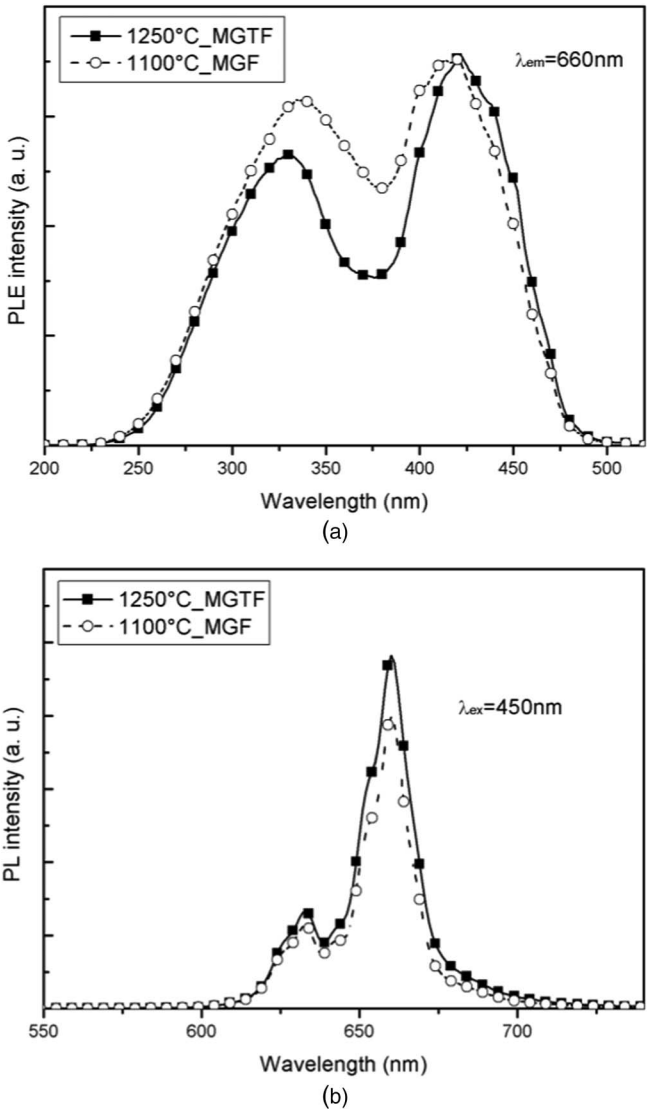

Figure 2. (a) PLE spectra (emission at 660 nm), (b) PL spectra (excitation at 450 nm) of samples prepared with and without Ti substitution at using different synthesis temperatures (1250°C_MGTF and 1100°C_MGF, respectively).

where E(λ)/hν, R(λ)/hν, and P(λ)/hν are the number of photons in the excitation source spectrum, the reflectance, and the emission of the phosphor, respectively.[25]

Figure 3 compares the photoluminescence intensities (excitation at 450 nm) of twelve samples with different Ge/Ti ratios ($Ge_{1-x}Ti_xO_2$, where x = 0, 0.05, 0.10, 0.15, 0.20, and 0.25) synthesized at 1100°C (open circles) or 1250°C (closed squares). Of the twelve samples, two samples contain the "1100°C_MGF" and "1250°C_MGTF" samples represented in Figures 1, 2a and 2b. Among the materials synthesized at 1100°C, maximal luminescence was observed when no Ti was substituted, and the photoluminescence intensity decreased as the Ti substitution ratio increased. In contrast, for the materials synthesized at 1250°C, the photoluminescence intensity tends to increase as the Ti substitution ratio increased, until x = 0.20, and then decreases. Among these samples, the sample with a Ge to Ti ratio of 4:1 synthesized at 1250°C showed the highest photoluminescence intensity.

Figure 4a shows XRD patterns of samples with various Ti substitution ratio synthesized at 1100°C. Figure 4b shows XRD patterns of samples with various Ti substitution ratio synthesized at 1250°C. All XRD patterns shown in Figures 4a and 4b appear similar to $Mg_{14}Ge_5O_{24}$ (PDF 01-071-0824) as shown in Fig. 1. In addition, some impurities such as SrF_2, Sr_2MgGeO_7, $SrTiO_3$, and MgO could

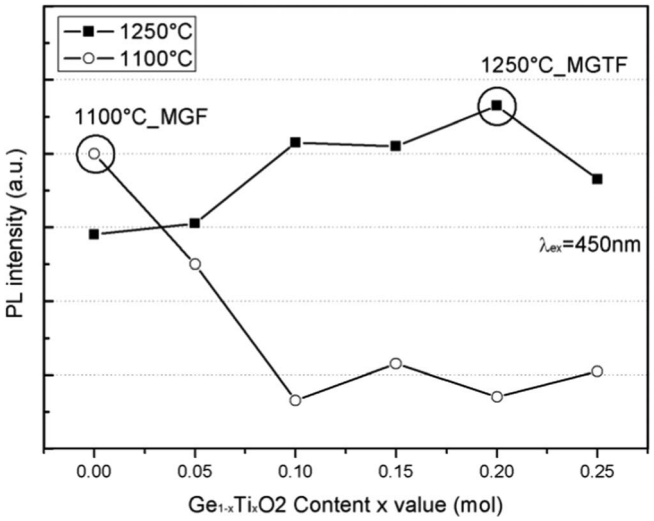

Figure 3. Comparison of photoluminescence intensities (excitation at 450 nm) of twelve samples with various Ti substitution ratios synthesized at 1100 or 1250°C.

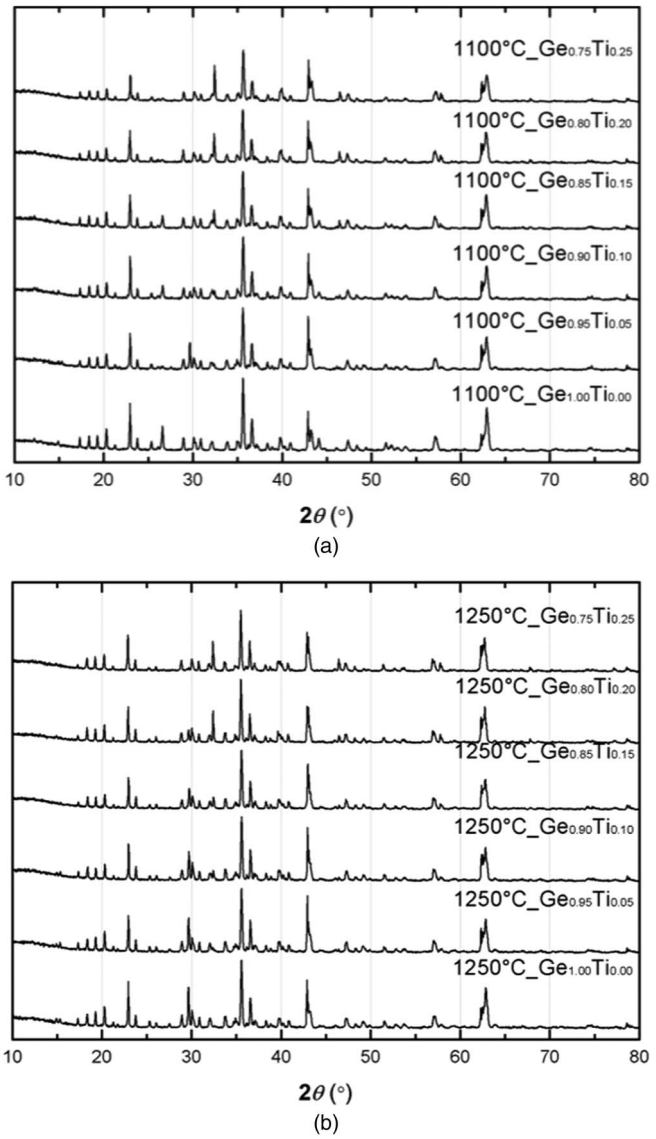

Figure 4. (a) XRD patterns of samples with various Ti substitution ratios synthesized at 1100°C, (b) XRD patterns of samples with various Ti substitution ratios synthesized at 1250°C.

be identified. The peaks of the impurities appeared weak. Among the impurities, MgO peak was observed in all samples at around 62°. We used a common peak of MgO as a tracer to suppress the error of XRD measurements.

Figures 5a–5c show PLE and XRD patterns for six samples synthesized at 1250°C. Six samples can be distinguished by the Ti substitution ratio. For example, the composition ratio of Ge and Ti at "1250_Ti_0.20" means Ge: Ti = 0.8: 0.2. We were able to observe a solid tendency on the XRD peak and the excitation spectrum. Figure 5a shows magnified and normalized XRD patterns (35°–36°) of samples with various Ti substitution ratios synthesized at 1250°C. Six samples of XRD data were normalized. We found a consistent trend that the XRD peak shifts to a lower angle as the Ti substitution ratio increases. For making a double check on the reliability of XRD measurement, the MgO impurities were traced. Figure 5b shows magnified and normalized XRD patterns (62°–63°) of samples with various Ti substitution ratios synthesized at 1250°C. We were able to observe the MgO phase as well as the germanate crystal phase. The MgO peak was observed at around 62°. Also, the XRD peak from the germanate crystal phase is found to be coexisted between 62.5 to 63°. XRD peaks from MgO phase tended to overlap at common positions. On the other hand, we have found that the peaks of germanate crystal phase tend to shift at lower angles as the Ti ratio increases. Based on the position peak of MgO, it could be confirmed that the germanate crystal might be distorted by Ti replacement at the Ge sites. Figure 5c shows normalized PLE spectra (emission at 660 nm) in the range of 350–520 nm. We could observe that the highest point of the excitation spectrum shifted from 418 to 422 nm. As the substitution ratio of Ti increases, the excitation spectrum tends to shift to the right. Among the six samples, "1250_Ti_0.20" sample have the best luminescence properties.

Figure 6 shows the XRD patterns of four samples obtained at two synthesis temperatures (1100 and 1250°C) and two Ti ratios ($Ge_{1.00}Ti_{0.00}$ and $Ge_{0.80}Ti_{0.20}$). The XRD patterns shown in Fig. 6 corresponds to those of 1100°C_$Ge_{1.00}Ti_{0.00}$, 1100°C_$Ge_{0.80}Ti_{0.20}$, 1250°C_$Ge_{1.00}Ti_{0.00}$, and 1250°C_$Ge_{0.80}Ti_{0.20}$ shown in Figs. 4a and 4b. As the dominant peaks were observed between 35° and 36°, the range of observation was limited to this region. As shown in Fig. 6, as the synthesis temperature increases, the peaks shift toward lower 2θ values, regardless of the Ti/Ge ratio. For samples synthesized at the same temperature, 1100 or 1250°C, the peaks shift toward lower 2θ values when Ti is substituted for Ge. To obtain a continuous shift trajectory of the peaks, we plotted a line connecting the peak maxima for the samples shown at the bottom and top of Fig. 6 (1100°C_$Ge_{1.00}Ti_{0.00}$ and 1250°C_$Ge_{0.80}Ti_{0.20}$, respectively). A comparison of these samples revealed a shift of 0.5° toward lower 2θ values. In previous studies, when Ti was substituted for a relatively large element, such as V, vanadium, a similar shift in the XRD pattern was observed.[26] Thus, we posited that the host crystal structure, $Mg_{14}Ge_5O_{24}$ (PDF 01-071-0824), is the same, but the unit volume is larger, unless there is a measurement error. Thus, partial substitution of TiO_2 could change the Mn^{4+}–O^{2-} bond length.

Figure 7 shows the Tanabe–Sugano energy diagram for the d^3 electron configuration in an octahedral crystal field. D_q on the x axis and E on the y axis are divided by B, the Racah parameter. The $^4T_1$ and $^4T_2$ excited states exhibit a linear relationship between the crystal field strength parameter (D_q) and energy (E). Therefore, if the crystal field strength (D_q) changes, the energy term (E) also changes. The excitation energy is known to be related to the crystal field strength,[27,28] according to the following relationship:

$$D_q = \left(3Ze^2 r^4\right) / \left(5R^5\right) \quad [2]$$

Here, D_q is the crystal field strength for a system with octahedral symmetry, R is the distance from the central ion and its ligand, Z is

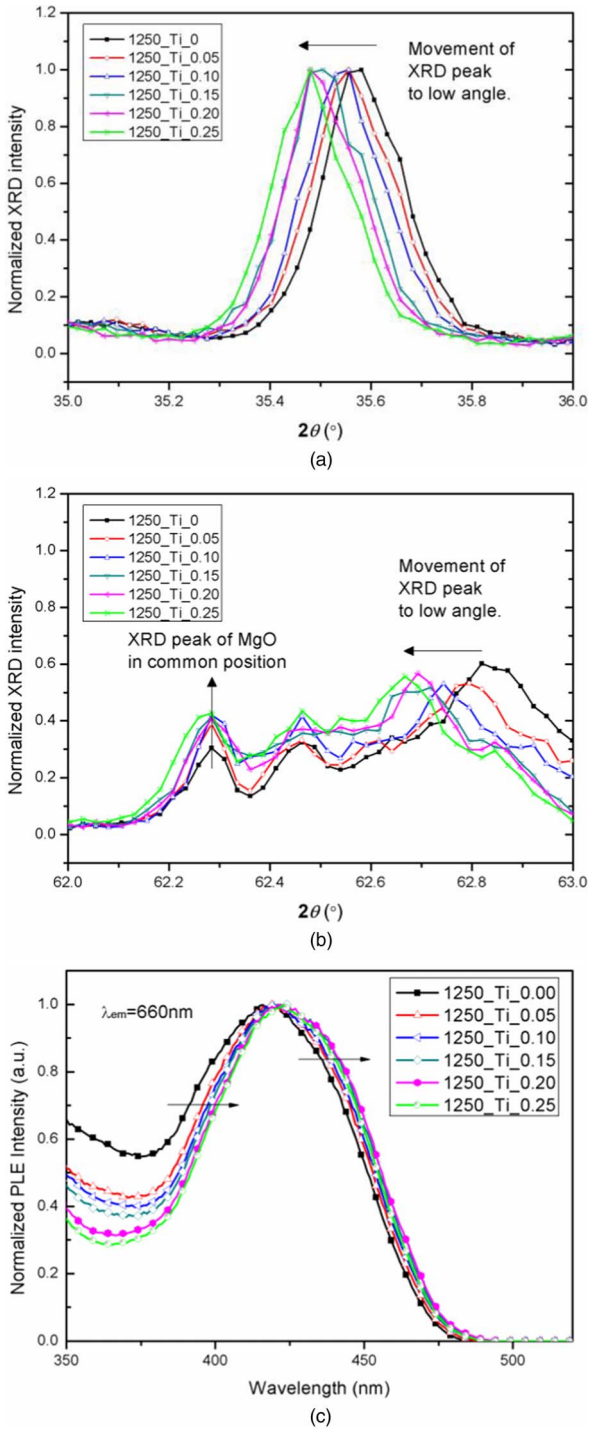

Figure 5. (a) Normalized XRD patterns (35°–36°) of the samples with various Ti substitution ratios synthesized at 1250°C, (b) Normalized XRD patterns (62°–63°) of the samples with various Ti substitution ratios synthesized at 1250°C, (c) Normalized PLE spectra (emission at 660 nm) over the range of 350–520 nm.

the charge or valence of the anion, E is the charge of the electron, and r is the radius of the d-wave function.

When an octahedral structure is formed with the same coordination, Ti^{4+} has a larger ionic radius than Ge^{4+}, and the bond length with O^{2-} is also longer. We believe that partial substitution of Ti for Ge may increase the bond length with O^{2-} in the octahedral structure into which Mn^{4+} could enter. Lengthening of the Mn^{4+}–O^{2-} bond in the six-fold coordination of the octahedral structure also decreases

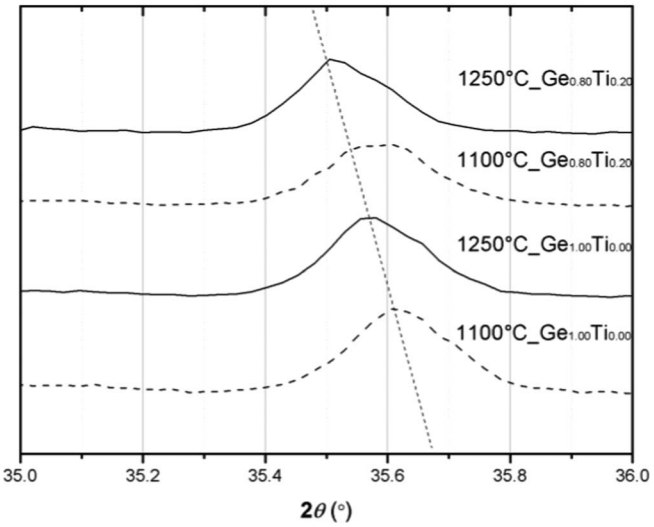

Figure 6. Magnified XRD patterns (35°–36°) of samples with Ti substitution ratios of 0 or 0.20 synthesized at 1000 or 1250°C (1100°C_$Ge_{1.00}Ti_{0.00}$, 1100°C_$Ge_{0.80}Ti_{0.20}$, 1250°C_$Ge_{1.00}Ti_{0.00}$, and 1250°C_$Ge_{0.80}Ti_{0.20}$).

the crystal field strength. In addition, this will result in a decrease in the energy level, bringing about shifts in the $^4T_1$ and $^4T_2$ energy levels of Mn^{4+}. As a result, a red-shifted $^4A_2 \rightarrow {}^4T_2$ absorption band is observed.

Increasing the synthesis temperature and partially substituting Ge with Ti resulted in a small redshift of the excitation band and a shift of the XRD pattern toward lower 2θ values. These observations imply that substitution with Ti caused crystal distortion.

Conclusions

In this work, we synthesized a deep-red-emitting Mn^{4+}-doped germanate phosphor. The internal quantum efficiency and the absorption ratio at 450 nm of the obtained phosphor, $3.5MgO\text{-}Ge_{1-x}Ti_xO_2\text{-}0.5MgF_2:Mn^{4+}$ (x = 0.2), were 45.36% and 50.16%, respectively. Substitution of Ge ions by Ti ions in the MGF:Mn^{4+} phosphor resulted in crystal distortion, which can affect the crystal field around Mn^{4+} ions. This variation in the crystal field is believed to be responsible for the observed redshift of the absorption band. As a result,

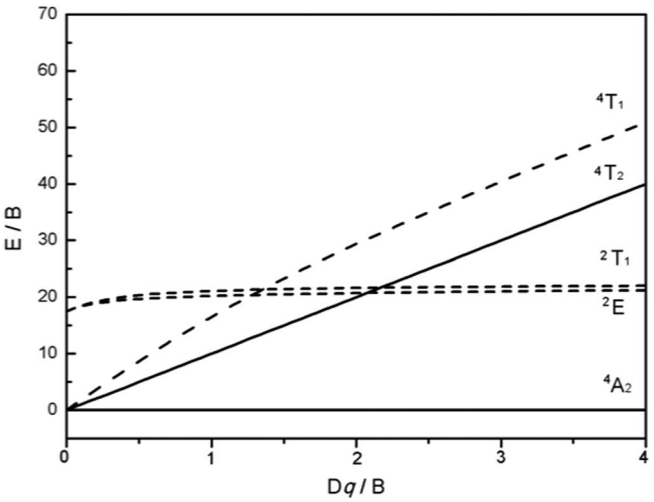

Figure 7. Tanabe–Sugano diagram for the d^3 electron configuration in an octahedral crystal field.

substitution with 20 mol% Ti improved the luminescence of Mn^{4+}-doped germanate phosphor by 19.3% when excited at 450 nm. Additional studies should be carried out to achieve further efficiency improvement. However, this deep-red-emitting germanate phosphor is applicable to wide color gamut white LEDs with K_2SiF_6:Mn^{4+} phosphors.

Acknowledgments

This research was supported by the Chung-Ang University Graduate Research Scholarship in 2016.

References

1. P. Pust, P. J. Schmidt, and W. Schnick, *Nat. Mater.*, **14**, 454 (2015).
2. M. S. Jang, Y. H. Choi, S. Wu, T. G. Lim, and J. S. Yoo, *J. Inf. Disp.*, **17**, 117 (2016).
3. M. Yamada, T. Naitou, K. Izuno, H. Tamaki, Y. Murazaki, M. Kameshima, and T. Mukai, *Jpn. J. Appl. Phys.*, **42**, L20 (2003).
4. J. Yang, Z. Quan, D. Kong, X. Liu, and J. Lin, *Cryst. Growth Des.*, **7**, 730 (2007).
5. C. Guo, D. Huang, and Q. Su, *Mater. Sci. Eng. B*, **130**, 189 (2006).
6. N. Avci, J. Musschoot, P. Smet, K. Korthout, A. Avci, C. Detavernier, and D. Poelman, *J. Electrochem. Soc.*, **156**, J333 (2009).
7. G. Anoop, K. P. Kim, D. W. Suh, I. H. Cho, and J. S. Yoo, *Electrochem. Solid-State Lett.*, **14**, J58 (2011).
8. W. B. Park, S. P. Singh, C. Yoon, and K.-S. Sohn, *J. Mater. Chem.*, **22**, 14068 (2012).
9. Y. Q. Li, J. E. J. van Steen, J. W. H. van Krevel, G. Botty, A. C. A. Delsing, F. J. DiSalvo, G. de With, and H. T. Hintzen, *J. Alloys Compd.*, **417**, 273 (2006).
10. K. Uheda, N. Hirosaki, Y. Yamamoto, A. Naito, T. Nakajima, and H. Yamamoto, *Electrochem. Solid-State Lett.*, **9**, H22 (2006).
11. P. F. Smet, A. B. Parmentier, and D. Poelman, *J. Electrochem. Soc.*, **158**, R37 (2011).
12. M. H. Du, *J. Lumin.*, **157**, 69 (2015).
13. M. G. Brik and A. M. Srivastava, *J. Lumin.*, **133**, 69 (2013).
14. P. Li, M. Peng, X. Yin, Z. Ma, G. Dong, Q. Zhang, and J. Qiu, *Opt. Express*, **21**, 18943 (2013).
15. M. Peng, X. Yin, P. A. Tanner, C. Liang, P. Li, Q. Zhang, J. Qiu, and A. Srivastava, *J. Am. Ceram. Soc.*, **96**, 2870 (2013).
16. Y. H. Jin, Y. H. Hu, H. Y. Wu, H. Duan, L. Chen, Y. R. Fu, G. F. Ju, Z. F. Mu, and M. He, *Chem. Eng. J.*, **288**, 596 (2016).
17. R. P. Cao, Z. H. Shi, G. J. Quan, T. Chen, S. L. Guo, Z. F. Hu, and P. Liu, *J. Lumin.*, **188**, 577 (2017).
18. R. P. Cao, D. Ceng, X. G. Yu, S. L. Guo, Y. F. Wen, and G. T. Zheng, *Funct. Mater. Lett.*, **8**, 4 (2015).
19. X. Ding, Q. Wang, and Y. Wang, *Phys. Chem. Chem. Phys.*, **18**, 8088 (2016).
20. S. P. Singh, M. Kim, W. B. Park, J. W. Lee, and K. S. Sohn, *Inorg. Chem.*, **55**, 10310 (2016).
21. J. H. Oh, H. Kang, Y. J. Eo, H. K. Park, and Y. R. Do, *J. Mater. Chem. C*, **3**, 607 (2015).
22. L. Thorington, *J. Opt. Soc. Am.*, **40**, 579 (1950).
23. S. Okamoto and H. Yamamoto, *J. Electrochem. Soc.*, **157**, J59 (2010).
24. Y. Lin-lin, Z. Xiao-Song, X. Jian-Ping, S. Jian, J. Han, L. Xiao-Juan, L. Lin-Lin, and L. Lan, *Chin. Phys. B*, **24**, 087802 (2015).
25. K. Ohkubo and T. Shigeta, *J. Illum. Eng. Inst. Jpn.*, **83**, 87 (1999).
26. Y. Wu, L. Fan, Q. Liu, S. Chen, W. Huang, F. Chen, G. Liao, C. Zou, and Z. Wu, *Sci. Rep.*, **5**, 9328 (2015).
27. J. Brgoch, C. K. Borg, K. A. Denault, A. Mikhailovsky, S. P. DenBaars, and R. Seshadri, *Inorg. Chem.*, **52**, 8010 (2013).
28. T.-W. Kuo, W.-R. Liu, and T.-M. Chen, *Opt. Express*, **18**, 1888 (2010).